

PACS numbers: 87.63.L–; 87.64.Cc
DOI: 10.1070/QE2013v043n08ABEH014973

Online quantitative analysis of multispectral images of human body tissues

S.A. Lisenko

Abstract. **A method is developed for online monitoring of structural and morphological parameters of biological tissues (haemoglobin concentration, degree of blood oxygenation, average diameter of capillaries and the parameter characterising the average size of tissue scatterers), which involves multispectral tissue imaging, image normalisation to one of its spectral layers and determination of unknown parameters based on their stable regression relation with the spectral characteristics of the normalised image. Regression is obtained by simulating numerically the diffuse reflectance spectrum of the tissue by the Monte Carlo method at a wide variation of model parameters. The correctness of the model calculations is confirmed by the good agreement with the experimental data. The error of the method is estimated under conditions of general variability of structural and morphological parameters of the tissue. The method developed is compared with the traditional methods of interpretation of multispectral images of biological tissues, based on the solution of the inverse problem for each pixel of the image in the approximation of different analytical models.**

Keywords: *mucosa, multispectral images, haemoglobin, oxygenation degree, diameter of capillaries, multiple regressions, analytical methods.*

1. Introduction

The effectiveness of cancer treatment is primarily dependent on the accuracy of the diagnosis in the early stages of development of a malignant tumour. In the respiratory tract and gastrointestinal tract, formation of precancerous lesions and early cancer usually occurs in the surface layers of the mucous membrane (hereinafter tissue), the total thickness of which is 200–500 μm [1].

Of all the existing methods for early diagnosis of tumours affecting the mucous membrane of hollow organs, including the respiratory and digestive tract, endoscopy still holds the lead. Contemporary endoscopic systems produce a high-resolution tissue image in real time directly on the computer display. However, images of the tissue in natural colour are affected by the anatomical features and spectral sensitivity of the endoscopic system, which prevents high diagnostic accuracy. In addition, conventional endoscopy is based on subjective assessment of images by a physician, based on his experience, expertise and emotional state (colour perception is reduced if the doctor is tired and enhanced if he is excited).

In the last decade image-enhanced endoscopy has been widely used in clinical practice [2, 3]. Its essence consists in the conversion of normal colour images of the tissue (by computer processing) into several spectral images, each of which corresponds to a specific wavelength of light – from violet (400 nm) penetrating into the surface layers of the tissue to red (700 nm) penetrating into deeper layers. This improves the visibility of blood vessels and other structures in the mucosa. However, such an endoscopy does not provide information about structural and morphological parameters (SMPs) of the tissue, which quantitatively characterise the development of pathology.

Structural and morphological parameters of mucous membranes can be quantitatively assessed by the methods of diffuse reflectance spectroscopy [4–12], which are based on the measurement of spectral and spatial characteristics of the light field scattered by a tissue and on the calculation of the sought-for quantities within the model of radiation transfer in the medium under study. For the practical implementation of these methods, use is made, as a rule, of fibre mini-probes, administered or embedded in the instrument channel of the endoscope. The main drawback of these measurements is their locality, because they allow one to judge the state of the tissue only at the point of contact with the end of the probe. Meanwhile, accurate and reliable endoscopic diagnosis requires information about the distribution of SMPs both in the suspicious lesion and in the surrounding area. In this sense, of higher diagnostic capability are the multispectral imaging methods of biological objects [13–20]. In these methods, the results of measurements of light scattered by a tissue are presented in the form of a $N_x \times N_y \times N_\lambda$ multilayer matrix, wherein each kth layer ($k = 1, \ldots, N_\lambda$) is a monochrome image with a spatial resolution $N_x \times N_y$, obtained in the kth spectral region. Until recently, the implementation of these methods required unique and expensive equipment, where high spectral resolution of the image was achieved at the expense of a significant increase in the duration of the measurements [13–16]. However, the advent of commercially available tunable liquid crystal filters [21, 22], allowing one to perform high-speed spectral selection of images, permitted similar measurements to be carried out on a much simpler instrumental base [17–20]. Currently, the only problem holding back the practical use of these methods in clinical practice is the large computational complexity of the quantitative analysis of multispectral images. Mapping the distribution of SMPs of a biological tissue involves the solution of the inverse problem for a large number of pixels of its multispectral image, the essence of which is to model the process of the light transport

S.A. Lisenko Belarusian State University, prosp. Nezavisimosti 4, 220050 Minsk, Belarus; e-mail: lisenko@bsu.by

Received 28 August 2012; revision received 7 March 2013
Kvantovaya Elektronika **43** (8) 777–784 (2013)
Translated by I.A. Ulitkin

in the tissue under study and to compare the calculated and experimental data. The known methods for calculating the light fluxes scattered by a tissue are either approximate and do not provide a sufficient accuracy, or involve large computational costs, and therefore exclude the possibility of real-time interpretation of experimental data. Moreover, stable solution of the inverse problem requires that the number of spectral layers of the image be several times greater than the number of model parameters, which further complicates the interpretation of the measurement results in real time.

In this paper we solve the problem of online processing of multispectral images of mucous membranes and obtain parametric maps characterising the development of pathology. It is already known that the growth of tumours greater than a few millimetres in diameter is possible only in the case of formation and germination of small capillaries that feed tumour cells with oxygen and nutrients [23]. As a result, a tumour tissue is different from a surrounding normal tissue by a higher hyperaemia and smaller blood vessels. Moreover, malignant neoplasms are characterised by intensive consumption of oxygen; therefore, the oxygen concentration in the vessels, diverting blood from the pathological areas, is typically below the normal level. In this regard, information about the distribution of haemoglobin concentration, the degree of blood oxygenation and diameters of blood vessels in the mucosa displayed on the screen during endoscopy could significantly improve the current early diagnosis of cancer.

2. Multispectral image processing algorithm for a biological tissue

The process of obtaining multispectral images of the tissue can be schematically represented as follows [17–19]. As a light source illuminating the tissue, a lamp or a 'white' light-emitting diode is used. A tunable optical filter placed in front of a radiation source 'cuts' from a wide spectrum of the emitter narrow spectral components, which are successively delivered via the optical fibre to the tissue. The light reflected from the tissue is collected by a lens on a CCD matrix, and a multispectral image of the tissue is formed on the basis of the matrix photosignals. To avoid glare in the tissue image, which arises due to the incidence of the reflected light on the light-sensitive elements, mutually orthogonal polarising filters are placed in front of the radiation source and the radiation detection unit. The light reflected from the tissue surface retains the initial polarisation and therefore is blocked by the filter in the recording channel. The remaining part of the light penetrates deep into the tissue and, as a result of multiple scattering, almost completely loses its original polarisation. The diffusely backscattered light passes through a polarising filter in the recording channel and is incident on the CCD matrix.

The signals at the CCD-matrix output (spectral image layers) are determined in accordance with the formula

$$V(x,y,\Lambda_k) = G(\theta,x,y)\int_{\lambda_1}^{\lambda_2} P(\lambda)F_k(\lambda)\tau(\lambda)D(\lambda)R(x,y,\lambda)\,\mathrm{d}\lambda, \quad (1)$$

where λ is the wavelength; x, y are the coordinates of the tissue surface element; $P(\lambda)$ is the power of the radiation source; $F_k(\lambda)$ is the transmittance of the tunable optical filter in the kth spectral region Λ_k ($k = 1,\ldots,N_\lambda$); $\tau(\lambda)$ is the transmittance of the optical fibre, polarisation filters and lenses; $D(\lambda)$ is the spectral sensitivity of the matrix; $R(x,y,\lambda)$ is the diffuse reflectance of the tissue, which is the ratio of the diffusely reflected radiation flux to the incident flux; $G(\theta,x,y)$ is the geometric factor which depends on the spatial distribution of the tissue illumination and the angle θ between the normal to the tissue surface and the axis of the collecting lens; and λ_1 and λ_2 are the boundary wavelengths by the detection unit.

Distributions of structural and morphological parameters $p(x,y)$ of mucosa are conveniently found based on the image $w(x,y,\Lambda_k) = V(x,y,\Lambda_k)/V(x,y,\Lambda_{\mathrm{ref}})$ obtained by normalising the original image $V(x,y,\Lambda_k)$ to one of its spectral layers $V(x,y,\Lambda_{\mathrm{ref}})$ (reference layer). It follows from (1) that the normalised image $w(x,y,\Lambda_k)$ is independent of the spatial distribution of the tissue illumination and the tissue position relative to the scattered radiation detection unit. In this connection, the dependence of $w(x,y,\Lambda_k)$ on the spectral characteristics of the components of the measuring device is easily taken into account based on the above measurement for the white diffuse reflector with the diffuse reflectance independent of Λ_k. When using narrow spectral regions, such measurements allow one to pass from the normalised tissue image $w(x,y,\lambda_k)$ to the normalised distributions of the diffuse reflectance of the tissue:

$$\frac{R(x,y,\lambda_k)}{R(x,y,\lambda_{\mathrm{ref}})} = \frac{w(x,y,\lambda_k)}{w_0(x,y,\lambda_k)},$$

where λ_k and λ_{ref} are centre wavelengths of the regions Λ_k and Λ_{ref}; and $w_0(x,y,\Lambda_k)$ is the normalised multispectral image of a white diffuse reflector.

Thus, the problem of determining the tissue SMP $p(x,y)$ can be reduced to the analysis of the spectral dependence of $r(x,y,\lambda_k) = R(x,y,\lambda_k)/R(x,y,\lambda_{\mathrm{ref}})$ for each point of the image. The proposed algorithm for solving this problem is the same for all points in the image; therefore, the dependence of the coefficients r and parameters p on the coordinates (x, y) will be omitted below for brevity. The spectral coefficients $r(\lambda_k)$ can be represented in the form of a measurement vector $\boldsymbol{r} = (r_k)$ with the $N_\lambda - 1$ component $r_k = -\ln r(\lambda_k)$. With a large number of spectral image layers it is convenient to use the method of principal components, the essence of which is to reduce the dimensionality of the original data and to select the most essential information. To this end, the vector $\boldsymbol{r}$ is expanded in the system of orthonormal basis vectors (principal components)

$$\boldsymbol{r} = \bar{\boldsymbol{r}} + \boldsymbol{G}\boldsymbol{\xi}, \quad (2)$$

where $\bar{\boldsymbol{r}}$ is the average measurement vector; $\boldsymbol{G} = (\boldsymbol{g}_1,\ldots,\boldsymbol{g}_T)$ is the matrix of size $(N_\lambda - 1) \times T$ with the columns of the main principal components $\boldsymbol{g}_n$ ($n = 1,\ldots,T$); T is the number of the principal component ($T = 1,\ldots,N_\lambda - 1$); and $\boldsymbol{\xi} = (\xi_1,\ldots,\xi_T)^{\mathrm{t}}$ are the expansion coefficients, which are found from the formula

$$\boldsymbol{\xi} = \boldsymbol{G}^{\mathrm{t}}(\boldsymbol{r} - \bar{\boldsymbol{r}}) \quad (3)$$

(t is the transposition operation).

As is known, the optimal approximation of a random vector $\boldsymbol{r}$ is the decomposition of its covariance matrix in eigenvectors [24, 25]

$$S_{ij} = \frac{1}{\sigma_i\sigma_j}\sum_{k=1}^{K}(r_i^k - \bar{r}_i)(r_j^k - \bar{r}_j), \quad (4)$$

where $\bar{\boldsymbol{r}} = (\bar{r}_i)$ and $\boldsymbol{\sigma} = (\sigma_i)$ are the mean value and variance of the vector $\boldsymbol{r}$, defined on the basis of the K ensemble of its realisations; and $1 \leqslant i, j \leqslant N_\lambda - 1$. Due to the rapid convergence of the expansion in question, the first principal components

(eigenvectors) corresponding to the largest eigenvalues of matrix (4) account for most of the variability of $\boldsymbol{r}$. Thus, we can significantly reduce the dimensionality of the experimental data and select several linearly independent components, which contain as much information as the original data. The number of linearly independent components is determined by analysing the eigenvalues l_T ($T = 1, \ldots, N_\lambda - 1$) of the covariance matrix of the coefficients $r(\lambda_k)$. To this end, its elements are divided by the number of spectral segments N_λ, resulting in the fulfilment of the condition $\sum l_T = 1$. Each of the eigenvalues of the resulting matrix determines the relative contribution of the corresponding eigenvector $\boldsymbol{g}_T$ to the variations of $\boldsymbol{r}$. The number of linearly independent components is determined by the number of the smallest eigenvalue for which $l_T > \delta r^2$ [25], where δr is the measurement error $r(\lambda_k)$.

Thus, to solve the inverse problem we may use not the coefficients $r(\lambda_k)$ directly measured in the experiment, but their linearly independent components obtained as projections of the measurement vector $\boldsymbol{r}$ to the space of its eigenvectors of the covariance matrix. The online method for solving such problems has been proposed in [26–29]. The method is based on the construction of explicit analytical expressions Y_p, relating the sought-for parameters of the medium, p, with the linearly independent components ($\boldsymbol{\xi}$) of the experimental data as $p = Y_p(\boldsymbol{\xi}, \boldsymbol{a}_p)$, where $\boldsymbol{a}_p$ is the vector of the parameters of the analytical expression. To construct the operators Y_p, the radiative transfer model is used in the medium under study, allowing one, for the given medium parameters, to calculate the measurement vector $\boldsymbol{r}$. On the basis of this model, a 'training' ensemble of realisations of p and $\boldsymbol{\xi}$ is formed, and the method of least squares coefficients is employed to determine the coefficients $\boldsymbol{a}_p$ of the selected analytical expressions. In most cases, the relationship between p and $\boldsymbol{\xi}$ is well described by polynomial regressions of the form [26–29]:

$$p = a_{00} \sum_{n=1}^{T} \sum_{m=1}^{M} a_{nm} (\xi_n)^m, \tag{5}$$

where M is the degree of the polynomial and a_{nm} are the regression coefficients. Regressions (5) allow any number of linearly independent coefficients to used for determining p, and the increase in M makes it possible to achieve an arbitrarily accurate approximation of the statistical relationship between p and $\boldsymbol{\xi}$ (although, as a rule, it is sufficient to use $M = 3$).

3. Optical model of a mucous membrane

The ensemble of SMP realisations and diffuse reflectance spectra of mucosa required to obtain an average measurement vector $\bar{\boldsymbol{r}}$, principal components ($\boldsymbol{g}_1, \ldots, \boldsymbol{g}_T$) and regression coefficients (5) is found on the basis of model calculations. In the framework of the model used, the radiative transfer process in a medium is described by its refractive index η, absorption coefficient k, mean cosine of the scattering indicatrix g and the transport scattering coefficient $\beta' = \beta(1 - g)$, where β is the scattering coefficient.

When the light flux falls on a biological tissue, part of this flux is reflected from the tissue surface due to the difference of the refractive index of light at the medium interface. Light penetrating deep into the tissue is scattered, and then repeatedly re-reflected between the inner layers and the tissue surface. In this connection, the surface layer of the tissue has a significant influence on the characteristics of its diffuse reflection. To take diffuse reflection into account, the refractive index of the tissue, η, is included in the number of the variable parameters of the model.

The spectrum $k(\lambda)$ is modelled as a linear combination of the absorption spectra of oxy- (HbO_2) and deoxyhaemoglobin (Hb), which are the major absorbers of light in the visible region of the spectrum [4–9, 14]:

$$k(\lambda) = \alpha(D_v, \lambda) f_v C_{tHb} \frac{\ln 10}{\mu_{tHb}} [S\varepsilon_{HbO_2}(\lambda) + (1 - S)\varepsilon_{Hb}(\lambda)], \tag{6}$$

where f_v is the volume concentration of capillaries; $C_{tHb} = 150$ g L^{-1} is the average concentration of haemoglobin in blood; $\mu_{tHb} = 64500$ g L^{-1} is the molar mass of haemoglobin; ε_{HbO_2} and ε_{Hb} are the molar absorption coefficients of HbO_2 and Hb [30]; S is the degree of blood oxygenation (the fraction of oxygenated haemoglobin in the total haemoglobin); and α is the correction factor that takes into account the difference between the absorptive capacities of haemoglobin evenly distributed over the tissue volume and haemoglobin localised in the capillaries [31, 32]. For randomly distributed capillaries of diameter D_v the coefficient α can be calculated from the equation [32]:

$$\alpha(D_v, \lambda) = 2\sqrt{3} \times \frac{1 - \exp[-\pi k_{tHb}(\lambda) D_v (1 - 0.043 k_{tHb} D_v)/2\sqrt{3}}{\pi k_{tHb}(\lambda) D_v}, \tag{7}$$

where $k_{tHb}(\lambda) = (C_{tHb} \ln 10/\mu_{tHb})[S\varepsilon_{HbO_2}(\lambda) + (1 - S)\varepsilon_{Hb}(\lambda)]$ is the absorption coefficient of haemoglobin.

The transport scattering coefficient of biological tissues in the visible region of the spectrum can be approximated with good accuracy by a power law [12, 33–35]

$$\beta'(\lambda) = C(\lambda_0/\lambda)^v, \tag{8}$$

where $\lambda_0 = 600$ nm; and $C = \beta'(\lambda_0)$ and v are the structural parameters of the tissue characterising the concentration and size of its 'effective' scatterers. To describe the single scattering indicatrix of the tissue, use is made of a one-parameter Henyey–Greenstein function [36, 37] with the scattering anisotropy factor g.

Thus, the optical model of a mucous membrane is determined by seven parameters: η, g, C, v, f_v, D_v and S. Below we present following ranges of variations in model parameters selected by analysing the results of various authors [4–12, 33–35, 38] for mucous membranes of the oral cavity, oesophagus, gastrointestinal tract and lungs.

The ranges of variations in the model parameters

η	1.35–1.45
g	0.5–0.95
C/mm^{-1}	.0.5–3.0
v	.0.3–2.0
f_v (%)	0.5–20
D_v/μm	4.5–75
S (%)	20–98

The diffuse reflectance of the tissue, $R(\lambda)$, is calculated using the Monte Carlo method [36, 37] in the range $\lambda = 450$–700 nm with a step in λ, equal to 10 nm ($N_\lambda = 26$), which approximately corresponds to the spectral resolution of modern tunable optical filters. The calculation was performed for a homogeneous medium by modelling random trajectories of 5×10^5 photons injected into the medium along the normal to

the surface. Varying the model parameters, the transport single scattering albedo of the medium $\Lambda' = \beta'/(k + \beta')$ for the wavelength of 632 nm should not go beyond the range of 0.5–0.98, corresponding to biological tissues.

4. Estimating the number of linearly independent components in the spectra of diffuse reflection

Based on the above model we formed an ensemble of 10^3 realisations of model parameters and corresponding vectors $\boldsymbol{r} = (r_k)$ with the components $r_k = -\ln r(\lambda_k)$, where $r(\lambda_k) = R(\lambda_k)/R(\lambda_{\text{ref}})$; $\lambda_{\text{ref}} = 700$ nm; and $k = 1, \ldots, N_\lambda - 1$. These data allow us to calculate the average measurement vector $\bar{\boldsymbol{r}}$ and eigenvectors $\boldsymbol{g}_n$ of its covariance matrix. Then, using formula (3) we can find projections $\boldsymbol{\xi}$ of all realisation of $\boldsymbol{r}$ onto the space of vectors $\boldsymbol{g}_n$ ($n = 1, \ldots, T$) and use the least squares method to obtain multiple regression coefficients a_{nm} between $\boldsymbol{\xi}$ and the model parameters p. However, it is first necessary to estimate the number of linearly independent components contained in $r(\lambda_k)$.

Analysis of the eigenvalues l_T of the covariance matrix of the coefficients $r(\lambda_k)$, shown in Fig. 1, demonstrates that at an error $\delta r \leqslant 4\%$ the measured coefficients $r(\lambda_k)$ contain five linearly independent components. This means that the first five eigenvectors $\boldsymbol{g}_n$ of the covariance matrix (4) listed in Table 1 allow any model realisation of $r(\lambda_k)$ to be approximated. The error of this approximation calculated by the formula

$$\delta_{\text{r}} = \frac{1}{N_\lambda - 1} \sum_{k-1}^{N_\lambda - 1} \frac{|r(\lambda_k) - r^*(\lambda_k)}{r(\lambda_k)},$$

where $N_\lambda = 26$ and $r^*(\lambda_k)$ is the approximation of $r(\lambda_k)$ by expression (2), does not exceed 4.7%.

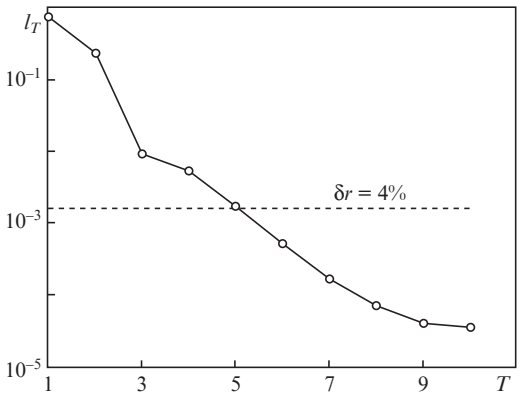

Figure 1. First ten eigenvalues of the covariance matrix of the coefficient $r(\lambda_k)$. The horizontal line corresponds to the $r(\lambda_k)$ measurement error of 4%.

It is of interest to estimate the approximation error of the experimental dependences $r(\lambda_k)$ with the help of the found principal components $\boldsymbol{g}_n$. For this purpose, use is made of the results of *in vivo* measurements of the diffuse reflectance spectra of the mucous membranes of the stomach and lungs, given in [11, 39]. Measurements were carried out by using a broadband light source, spectrophotometer and optical fibres delivering the exciting radiation from the source to the tissue and the radiation scattered by the tissue to spectrophotometer. Because during the endoscopy it is difficult to follow the identical measurement conditions for the tissue under examination and the calibration sample, the diffuse reflectance of the tissue, R_{exp}, is defined up to a constant factor. This is evident in the fact that the experimental coefficients of $R_{\text{exp}}(\lambda)$, shown in Fig. 2, in some cases, exceed unity. However, for the purposes of this work of interest is the relative spectral variation in the diffuse reflectance of the tissue.

Table 1. Average measurement vector $\bar{\boldsymbol{r}}$ and eigenvectors $\boldsymbol{g}_n$ of its covariance matrix.

λ_k/nm	$\bar{\boldsymbol{r}}$	$\boldsymbol{g}_n$				
		$n = 1$	$n = 2$	$n = 3$	$n = 4$	$n = 5$
450	2.2809	0.2169	−0.0887	0.5324	0.4289	0.5408
460	1.7752	0.2065	−0.1774	−0.0950	0.3175	−0.0867
470	1.5756	0.2016	−0.1929	−0.2379	0.2615	−0.1538
480	1.4664	0.2017	−0.1916	−0.2954	0.2121	−0.1313
490	1.4673	0.2074	−0.1722	−0.2781	0.1603	−0.0525
500	1.5018	0.2159	−0.1375	−0.2259	0.1102	0.0761
510	1.5779	0.2218	−0.1060	−0.1513	0.0577	0.1486
520	1.7406	0.2229	−0.1014	−0.0515	0.0028	0.1074
530	2.0215	0.2187	−0.1269	0.1074	−0.0312	−0.0755
540	2.2058	0.2167	−0.1327	0.2442	−0.0525	−0.1521
550	2.1928	0.2212	−0.1043	0.2683	−0.1115	−0.0262
560	2.1252	0.2248	−0.0756	0.2458	−0.1727	0.0535
570	2.1906	0.2184	−0.1216	0.2210	−0.2047	−0.2057
580	2.1993	0.2136	−0.1461	0.1814	−0.2334	−0.3942
590	1.6536	0.2272	−0.0454	−0.0441	−0.3623	−0.0144
600	0.9964	0.2216	0.1012	−0.1445	−0.2964	0.1575
610	0.6885	0.2109	0.1609	−0.1539	−0.2148	0.1617
620	0.4823	0.2050	0.1849	−0.1678	−0.1457	0.1675
630	0.3569	0.1906	0.2308	−0.1205	−0.0562	0.1413
640	0.2757	0.1747	0.2691	−0.0662	0.0105	0.0793
650	0.2167	0.1639	0.2904	−0.0320	0.0403	0.0425
660	0.1620	0.1528	0.3092	0.0084	0.0767	−0.0035
670	0.1151	0.1424	0.3247	0.0380	0.1001	−0.0422
680	0.0701	0.1284	0.3424	0.0912	0.1432	−0.1381
690	0.0275	0.1091	0.3599	0.1413	0.3008	−0.5086

The experimental spectra $R_{\text{exp}}(\lambda)$ of the mucous membranes of the stomach were interpolated to the values of λ, corresponding to the vectors $\boldsymbol{g}_n$ (Table 1) and were normalised to $R_{\text{exp}}(\lambda_{\text{ref}} = 7000$ nm) to obtain the vectors $\boldsymbol{r}$. Next, formula (3) was used to calculate the projections of $\boldsymbol{r}$ onto the space of the vectors $\boldsymbol{g}_n$ ($n = 1, \ldots, 5$) and equation (2) was employed to approximate the dependences $R_{\text{exp}}(\lambda)/R_{\text{exp}}(\lambda_{\text{ref}})$. The results of the approximation, along with the experimental dependences of $R_{\text{exp}}(\lambda)$, are shown in Fig. 2a. The error δ_{r} for different spectra ranges from 1.3% to 2.6%, which is consistent with the model estimates.

The diffuse reflectance spectra of the mucous membrane of the lungs are given in [11] for the range $\lambda = 475$–675 nm. This range is narrower than that used in the simulation (400–700 nm). Therefore, in this case, all model realisation of $R(\lambda)$ were interpolated to λ, corresponding to the experimental data, and were normalised to $R(\lambda_{\text{ref}} = 675$ nm). The data obtained allowed us to calculate the vectors $\bar{\boldsymbol{r}}$ and $\boldsymbol{g}_n$, used to approximate the experimental dependences $R_{\text{exp}}(\lambda)/R_{\text{exp}}(\lambda_{\text{ref}})$. The corresponding approximation errors amount to 3.9% for normal tissues and 5.0% for tumours (Fig. 2b). The latter value is slightly greater than the upper limit of δ_{r} for the simulated data, but taking into account the measurement error and digitisation of experimental data, as well as discrepancies in the wavelengths used in the experiment and model calculations, this fact is quite natural.

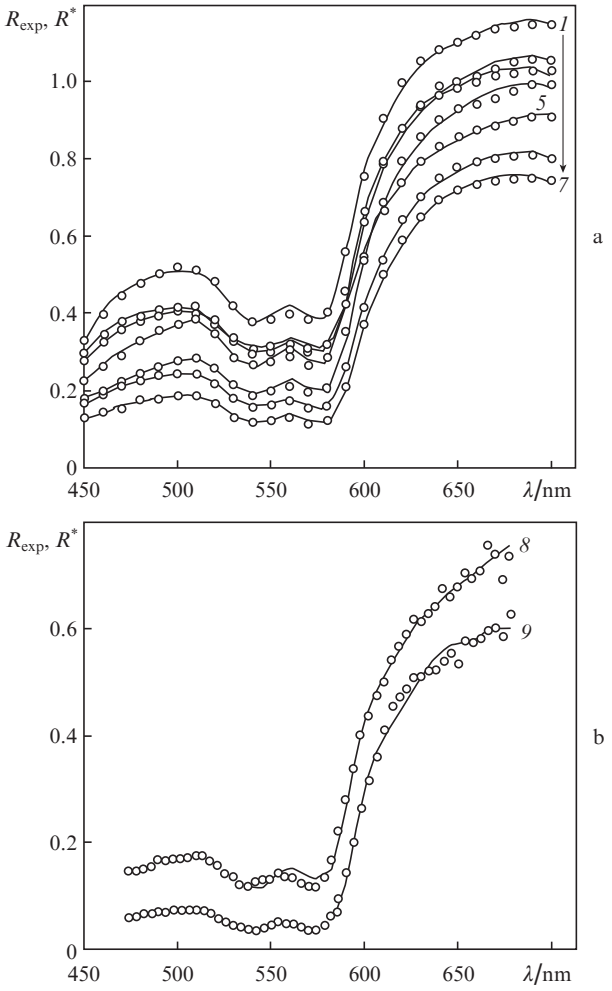

Figure 2. Approximation of the experimental diffuse reflectance spectra of mucous membranes of (a) stomach and (b) lungs using the five principal components; points are the experimental data, curves are the results of calculations by formulas (2), (3). The arrow denotes the direction of the spectrum numbering.

5. Analysis of the model parameter retrieval errors

Errors in retrieval of the model parameters p from the spectral coefficients $r(\lambda_k)$ are estimated by the closed numerical experiment, the essence of which is as follows. For each of the simulated realisation of $r(\lambda_k)$, p is calculated using formulas (3) and (5) by superimposing random deviations within δr on $r(\lambda_k)$ (simulating the optical measurement errors). The resulting value of the parameter p^* is compared with its value for the given realisation. After going through all realisations, the average parameter retrieval error δ_p is calculated.

The results of the above analysis allow the following conclusions to be drawn. Assuming that the model parameters exhibit total variability (their values are not rigidly fixed) in the spectral coefficients $r(\lambda_k)$, one can determine the degree of blood oxygenation S, the average diameter of capillaries D_v and the dimensionless parameter v, which characterises the average size of tissue scatterers and determines the spectral behaviour of its coefficient $\beta'(\lambda)$. As for the total haemoglobin concentration in the tissue $F_{tHb} = f_v C_{tHb}$ (g L^{-1}) – the most important parameter in the diagnosis of cancer, the informativeness of its retrieval (the ratio of the average retrieval error to the *a priori* uncertainty) is close to unity. The same applies to the model parameter C, which is a function of the concentration of the scattering centres and the refractive index of the tissue. The reason for this is the ambiguity of the inverse problem solution because it is impossible to separate the contributions of absorption and scattering coefficients into the coefficients $r(\lambda_k)$. In this regard, one can retrieve from $r(\lambda_k)$ only the ratio F_{tHb}/C or $F_{tHb}/\beta'(\lambda)$, where λ lies within the range used by the multispectral tissue imaging system. Fortunately, for most biological tissues we have reliable data on the coefficient $\beta'(\lambda)$, obtained in the laboratory conditions by the integrating sphere spectrophotometry [12, 33–35]. It should be also noted that for each type of the tissue $\beta'(\lambda)$ varies within a comparatively small limit. Thus, according to data from [12, 34], for normal stomach tissues and pathological lesions of various forms β' (600 nm) lies in the range from 1.73 to 2.4 mm^{-1}. For normal and tumoured lung tissues β' (632 nm) = 1.02–1.24 [33]. This suggests that in the presence of *a priori* information about the type of the biological tissue, the measured coefficients $r(\lambda_k)$ can also help to determine the haemoglobin concentration in the tissue.

Regression coefficients (5) for the parameters F_{tHb}/C, S, D_v and v are listed in Tables 2–5. One can judge the accuracy of the estimates of these parameters by the diagrams shown in Fig. 3, in which the known values of the parameters p are compared with the values of p^*, retrieved from the coefficients $r(\lambda_k)$ at $\delta r = 2\%$.

Consider the examples of retrieval of SMPs of mucous membranes from the experimental spectra of their diffuse reflection, presented in Fig. 2. The diffuse reflectance spectra corresponding to the stomach tissue were interpreted on the

Table 2. Regression coefficients a_{nm} (5) for $p = \ln(F_{tHb}/C)$ ($a_{00} = 1.8724$).

m	n		
	1	2	3
1	0.4492	−0.0359	0.0047
2	−0.3411	0.0605	0.0269
3	−0.9042	0.2076	−0.1318
4	−1.3445	0.1198	0.2126
5	0.1033	−0.2700	−0.0668

Table 3. Regression coefficients a_{nm} (5) for $p = \ln(F_{tHb}/C)$ ($a_{00} = 0.5650$).

m	n		
	1	2	3
1	−0.2187	0.0212	−0.0011
2	−0.5705	−0.1322	−0.0183
3	−0.1272	0.0479	−0.0118
4	−0.0766	0.1036	−0.0264
5	−0.3603	−0.1485	0.0737

Table 4. Regression coefficients a_{nm} (5) for $p = D_v$ ($a_{00} = 34.982$).

m	n		
	1	2	3
1	−5.9109	−2.3654	0.0846
2	−68.526	4.2881	0.3785
3	−108.20	35.430	−11.785
4	−68.642	−0.4489	5.5019
5	64.935	−12.348	23.519

Table 5. Regression coefficients a_{nm} (5) for $p = v$ ($a_{00} = 1.1176$).

m	n		
	1	2	3
1	−0.5089	0.0387	−0.0012
2	−0.8043	−0.0379	0.0063
3	0.7425	−0.2666	0.0947
4	−2.8033	−0.1219	0.6794
5	−1.8777	−0.5878	0.5382

basis of formulas (3) and (5) with the vectors $\bar{\boldsymbol{r}}$, $\boldsymbol{g}_n$ and coefficients a_{nm} from Tables 1–5. To assess the SMPs of the lung tissue we used the same formulas, but with the vectors $\bar{\boldsymbol{r}}$, $\boldsymbol{g}_n$ and coefficients $a_{\rm nm}$ corresponding to the spectral range 475 to 675 nm. The parameters $F_{\rm tHb}$, S, $D_{\rm v}$ and v, retrieved from the experimental dependences $R_{\rm exp}(\lambda)/R_{\rm exp}(\lambda_{\rm ref})$ (where $\lambda_{\rm ref}$ is the right boundary of the spectral range), are listed in Table 6 [according to the numeration of the $R_{\rm exp}(\lambda)$ spectra in Fig. 2]. The haemoglobin concentrations in the tissue are obtained by assuming that C is constant for each type of the tissue (1.39 $\rm mm^{-1}$ for lungs [33], and 1.74 $\rm mm^{-1}$ for stomach [34]). Unfortunately, the exact values of the tissue parameters corresponding to the experimental data are not known; therefore, it is impossible to draw conclusions about the accuracy of their quantitative assessment. However, the parameters obtained quantitatively characterise the structure and bio-

Table 6. Structural and morphological parameters of the mucous membranes of the stomach (Nos 1–7) and lungs (Nos 8, 9; Fig. 2b), retrieved from the experimental diffuse reflectance spectra.

No	$F_{\rm tHb}$/g $\rm L^{-1}$	S	$D_{\rm v}$	v
1	1.9	0.77	45	0.39
2	2.7	0.89	49	0.03
3	2.7	0.83	57	0.55
4	4.9	0.91	62	0.11
5	2.5	0.68	65	0.76
6	5.6	0.91	65	1.02
7	7.5	0.96	66	0.94
8	3.8	0.94	60	0.39
9	6.4	0.94	41	0.29

chemical composition of the tissue and hence the maps of their distributions in the mucous membranes under various pathological conditions can be used for impartial quantitative description of these pathologies.

Of interest is to note the significant differences between the found values of the haemoglobin concentration and capillary diameter for normal and tumoured lung tissues. These differences are in good agreement with the morphological changes in the tissue caused by the angiogenesis process [23] (active growth of small capillaries in the tumour). With regard to the degree of blood oxygenation, it is identical in both cases. However, to verify the pathology, of importance is not a specific value of this parameter but its distribution in the

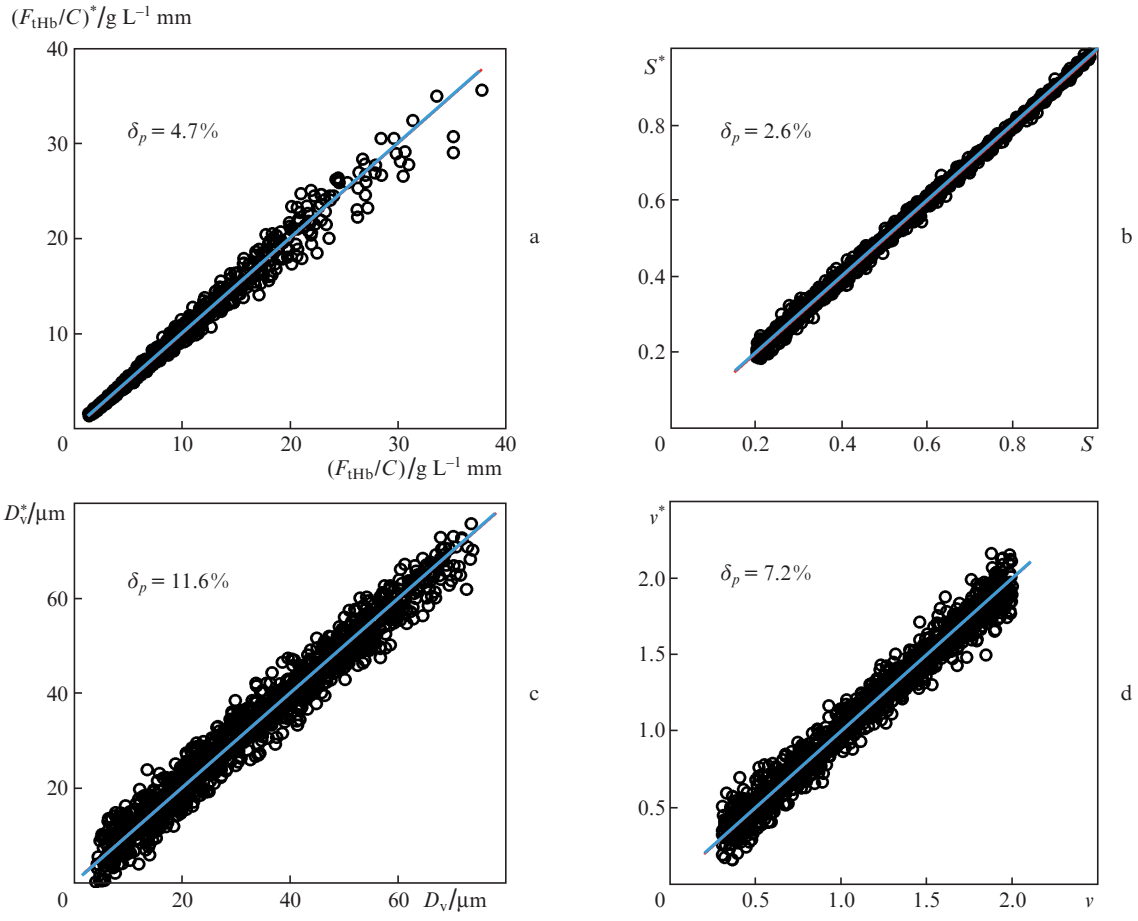

Figure 3. Results of closed numerical experiments on retrieval of the parameters (a) $F_{\rm tHb}/C$, (b) S), (c) $D_{\rm v}$ and (d) v using the five principal components of $r(\lambda_k)$ with $\delta r = 2\%$; δ_p is the average parameter retrieval error.

vascular branches delivering/diverting blood to/from a suspicious neoplasm.

6. Comparison with analytical methods

Traditional methods of analysis of multispectral images of biological tissues are based on the determination of the spectral values of the diffuse reflectance of the tissue (up to a constant factor) for each point of its image and on the solution of the inverse problem in the approximation of various numerical or analytical models [14, 15, 18–20, 38, 40]. In this case, the same procedure (calculation of the diffuse reflectance of the medium simulating a biological tissue) is repeated many times. Obviously, the overall image processing time depends on the speed of this procedure. In this connection, very popular among the researchers are various analytical methods of radiation transfer theory, giving the final result in a simple analytic form [14, 15,18–20, 40].

Consider the evaluation of the retrieval accuracy of the SMPs of the tissue using the most popular analytical methods for calculating diffuse reflectance, as well as the required computer time. Without getting to the essence of the methods and assumptions used in them, we give only the basic formulas (for more details we refer the reader to papers listed below).

1. Engineering methods of radiation transfer theory, developed at the Institute of Physics of the National Academy of Sciences of Belarus [41, 42], yield for the diffuse reflectance of a homogeneous medium illuminated by a directed light beam the expression:

$$R = \frac{(1-f)(1-f^*)R_0}{1-f^*R_0^*}, \tag{9}$$

where f and f^* are the reflection coefficients from the surface of a medium during its outside and inside illumination;

$$R_0 = \exp\left(-\frac{36}{7}\sqrt{\frac{k}{3\varepsilon'}}\right), \quad R_0^* = \left(-4\sqrt{\frac{k}{3\varepsilon'}}\right)$$

are the reflection coefficients of a medium without an external border in the case of directed and diffuse illumination, respectively; $\varepsilon' = k(1-g) + \beta'$ is the effective attenuation coefficient.

2. In the framework of the diffusion approximation of radiation transfer theory [43] the diffuse reflectance of a medium can be calculated by using the expression

$$R = 0.5\Lambda'\left[1+\exp\left(-\frac{4A}{3}\right)\sqrt{3(1-\Lambda')}\right]\exp[-\sqrt{3(1-\Lambda')}], \tag{10}$$

where Λ' is the transport single scattering albedo; and $A = (1+f^*)/(1-f^*)$.

3. Two-stream theory of Kubelka–Munk [44] describes the process of the radiation transfer in a medium with the use of two empirical coefficients (K and S) depending on the absorbing and scattering properties of the medium. For known values of these coefficients, the diffuse reflectance of a medium can be calculated by the formula

$$R_0^* = \left[1+\frac{K}{S}\left(1+\sqrt{1+\frac{2S}{K}}\right)\right]^{-1}. \tag{11}$$

Burger et al. [45] showed that when the medium is illuminated along the normal to its surface, one can use $0.27\beta'/k$ instead of the ratio S/K. To account for light reflection from the medium surface, we will use formula (9), where $R_0 = R_0^*$.

4. Based on the Monte Carlo method, Jacques [46] obtained a simple analytical expression relating the diffuse reflectance of a homogeneous medium with its optical parameters k and β':

$$R = A\exp\left[\frac{-7.8}{\sqrt{3(1-\beta'/k)}}\right], \tag{12}$$

where A is a constant, the value of which is not essential for the analysis of the relative spectral variation in $R(\lambda)$.

Substituting expressions (6)–(8) for the coefficients k and β' into formulas (9)–(12) we obtain the model dependence of the diffuse reflectance of mucosa on λ and the parameters η, g, C, v, f_v, D_v and S. Then, using the least-squares method we can calculate the values of these parameters corresponding to the minimum difference between the experimental and model diffuse reflectance spectra of the tissue. The effectiveness of these analytical models can be estimated on the basis of the analysis of the diffuse reflectance spectra calculated numerically by the Monte Carlo method – the most accurate method for solving the radiation transfer equation, which has no restrictions on the optical parameters of the medium. For this purpose, we used the previously obtained ensemble of 10^3 realisations of model parameters p and their respective coefficients $r(\lambda_k) = R(\lambda_k)/R(\lambda_{ref})$ ($k = 1, \ldots, 25$; $\lambda_{ref} = 700$ nm). We introduced random errors (within 2%) in the spectra $r(\lambda_k)$ and selected the parameters p in the approximation of the above analytical models. The found values of the model parameters were compared with the values corresponding to the spectra $r(\lambda_k)$.

The average retrieval errors of the parameters F_{tHb}/C, S, D_v and v are given in Table 7. It can be seen that the most accurate estimates of the sought-for parameters correspond to model 1 (according to the above numbering). However, their comparison with similar errors for the regression model (Fig. 3) showed that the accuracy of evaluation of any of the model parameters did not increase. Model 4 allows one to obtain satisfactory estimates of the parameters S, F_{tHb}/C and v, which however are much less accurate than those obtained with the regression model. This is apparently caused by an insufficiently accurate description of the radiation transfer process by analytical model 4. As shown in [40], the results of calculations by formula (12) are in good agreement with the experimental data only for media with $\Lambda' > 0.94$. Meanwhile, the variations of the model parameters listed in Section 3 correspond to a much wider range of Λ' values – from 0.1 to 0.99. As for models 2 and 3, they are, as seen from these results, practically unsuitable for quantitative analysis of the diffuse reflectance spectra of mucous membranes (at least in the spectral range).

Table 7. Average retrieval error of the model parameters.

Model	$\delta(F_{tHb}/C)$ (%)	δS (%)	δD_v (%)	δv (%)
1	6.9	3.0	15.5	9.0
2	144	13.4	35	37
3	58	12.1	46	26.8
4	15.6	4.1	34	12.71

Consider the evaluation of computer time needed to solve the inverse problem in the framework of the regression and analytical models. For a computer with the Intel Core i7-860 processor (2.8 GHz), the average curve fitting time for $r(\lambda_k)$ consisting of 25 points λ_k in the approximation of the above analytical models is 0.42–0.79 s (the shortest time corresponds to model 1, the longest – to model 2). Calculation of the model parameters based on their regression relation with

$r(\lambda_k)$, i.e. by formulas (3) and (5), is $\sim 2.3 \times 10^{-5}$ s. It is easy to calculate, in the first case, the average processing time of 25 normalised spectral layers of images with a resolution of 250×250 pixels will be 7 to 14 hours. If use is made of the regression model, the process of obtaining distribution maps of the parameters F_{tHb}/C, S, D_v and v will take only 1.45 s, which suggests the possibility of monitoring (important for oncology) parameters of mucous membranes in near real-time.

Thus, the elaborated method allows one to obtain near real-time maps of the distributions of the tissue parameters characterising the process of pathology development. This method may advantageously be used in the course of endoscopic examination of mucous membranes of mouth, oesophagus, gastrointestinal tract and lungs. The data obtained by this method permit passing from the subjective (visual) study of the mucous membrane to an objective (quantitative) assessment of its condition and significantly reducing the chance of misdiagnosis.

References

1. Gallinger Yu.I., Godzhello E.A. *Operativnaya endoskopiya pishchevoda* (Operative Endoscopy of Oesophagus) (Moscow: RNTsKh RAMN, 1999) p. 273.
2. Takahira M., Kawata M., Suzuki I. Pat. US № 2012/0086790 A1, 12.04.2012.
3. Osawa H., Yoshizawa M., et al. *Gastrointestinal Endoscopy*, **67**, 2 (2008).
4. Zonios G., Perelman L.T., et al. *Appl. Opt*., **38**, 31 (1999).
5. Amelink A., Bard M.P., Burgers S.A., Sterenborg H.J. *Appl. Opt*., **42**, 19 (2003).
6. Bigio I.J., Bown S.G. *Cancer Biol. Therapy*, **3**, 3 (2004).
7. Bargo P.R., Prahl S.A., et al. *J. Biomed. Opt*., **10**, 3 (2005).
8. Palmer G.M., Ramanujam N. *Appl. Opt*., **45**, 5 (2006).
9. Stratonnikov A.A., Meerovitch G.A., Ryabov A.V., Savel'eva T.A., Loshchenov V.B. *Kvantovaya Elektron*., **36**, 1103 (2006) [*Quantum Electron*., **36**, 1103 (2006)].
10. Reif R., Amorosino M.S., et al. *J. Biomed. Opt*., **13**, 1 (2008).
11. Zeng H., Fawzy Y.S. Pat US № 2009/0270702 A1; Int. Cl. A61B 5/1455, A61B 6/00; 29.10.2009.
12. Giraev K.M., Ashurbekov N.A., Lakhina M.A. *Zh. Prikl. Spektrosk*., **78**, 104 (2011).
13. Hammer M., Schweitzer D., Thamm E., Kolb A. *Int. Ophthalmol*., **23**, 291 (2001).
14. Yu C.C., Lau C., O'Donoghue G., et al. *Opt. Express*, **16**, 20 (2008).
15. Jacques S.L. *J. Innovat. Opt. Health Sci*., **2**, 2 (2009).
16. Tseng T.Y., Lai P.J., Sung K.B. *Opt. Express*, **19**, 2 (2011).
17. Chen C., Jacobs K.M., Lu J.Q., Cuenca R.E., Finley J., Hu X.H. *PIERS Online*, **3**, 6 (2007).
18. Jakovels D., Spigulis J. *J. Biophoton*., **3**, 3 (2010).
19. Jacques S.L., Samatham R., Choudhury N. *Biomed. Opt. Express*, **1**, 1 (2010).
20. Bersha K.S. *Master Thesis Report* (Univ. Eastern Finland, 2010) p. 58.
21. Gat N. *Proc. SPIE Wavelet Applications VII*, **4056**, 1 (2000).
22. Hardeberg J.Y., Schmitt F., Brettel H. *Opt. Eng*., **41**, 10 (2002).
23. Prozorovskii V. *Nauka i zhizn'*, (9), 9 (2006).
24. Zuev V.E., Komarov V.S. *Statisticheskie modeli temperatury i gazovykh component zemnoi atmosfery* (Statistical Models of Temperature and Gas Components of the Earth's Atmosphere) (Leningrad: Gidrometeoizdat, 1986) p. 264.
25. Veselovskii I., Kolgotin A., Müller D., Whiteman D.N. *Appl. Opt*., **44**, 25 (2005).
26. Kugeiko M.M., Lisenko S.A. *Zh. Prikl. Spektrosk*., **74**, 650 (2007).
27. Lisenko S.A., Kugeiko M.M. *Issledovanie Zemli iz kosmosa*, (6), 21 (2011).
28. Lisenko S.A., Kugeiko M.M. *Zh. Prikl. Spektrosk*., **79**, 932 (2012).
29. Lisenko S.A., Kugeiko M.M. *Opt. Spektrosk*., **114**, 105 (2013) [*Opt. Spectrosc*., **114**, 251 (2013)].
30. Prahl S.A. http://omlc.ogi.edu/spectra/hemoglobin/index.html.
31. Verkruysse W., Lucassen G.W., de Boer J.F., Smithies D.J., Nelson J.S., van Gemert M.J.C. *Phys. Med. Biol*., **42**, 1 (1997).
32. Barun V.V., Ivanov A.P. *Opt. Spektrosk*., **96**, 940 (2004) [*Opt. Spectrosc*., **96**, 1019 (2004)].
33. Qu J., MacAulay C., Lam. S., Palcic B. *Appl. Opt*., **33**, 31 (1994).
34. Bashkatov A.N. et al. *Med. Laser Application*, **22**, 95 (2007).
35. Wei H.J., Xing D., Lu J.J., et al. *Gastroenterol*., **11**, 16 (2005).
36. Prahl S.A. *PhD Thesis* (Univ. Texas at Austin, 1988) p. 221.
37. Wang L. et al. *Comput. Meth. Progr. Biomed*., **47**, 131 (1995).
38. Hidović-Rowe D., Claridge E. *Phys. Med. Biol*., **50**, 1071 (2005).
39. *Atlas of Spectral Endoscopic Image*s (Japan: Chiba Univ. Hospital, 2008) p. 68.
40. Fabbri F., Franceschini M.A., Fantini S. *Appl. Opt*., **42**, 16 (2003).
41. Zege E.P., Ivanov A.P., Katsev I.L. *Perenos izobrazhenii v rasseivayushchei srede* (Image Transfer in a Scattering Medium) (Minsk: Nauka i Tekhinka, 1985) p. 327.
42. Ivanov A.P., Barun V.V. *Opt. Spektrosk*., **104**, 344 (2008).
43. Farrell T.J., Patterson M.S., Wilson B.C. *Med. Phys*., **19**, 4 (1992).
44. Egan W.G., Hilgerman T.W. *Optical Rroperties of Inhomogeneous Materials* (New York: Acad. Press, 1979) p. 246
45. Burger T., Ploss H.J., Kuhn J., et al. *Appl. Spectrosc*., **51**, 5 (1997).
46. Jacques S.L. http://omlc.ogi.edu/ news/may99/rd/index.html (1999).